Depósito de investigación de la Universidad de Sevilla

https://idus.us.es/

This is an Accepted Manuscript of an article published by IEEE Transactions on Industrial Electronics on 12/07/2019, available at: https://doi.org/10.1109/TIE.2017.2714126

"© 2018 IEEE. Personal use of this material is permitted. Permission from IEEE must be obtained for all other uses, in any current or future media, including reprinting/republishing this material for advertising or promotional purposes, creating new collective works, for resale or redistribution to servers or lists, or reuse of any copyrighted component of this work in other Works"

Model Predictive Control of Six-phase Induction Motor Drives Using Virtual Voltage Vectors

I. Gonzalez-Prieto, M.J. Duran, J.J. Aciego, C. Martin, F. Barrero, *Senior Member, IEEE*

***Abstract*– The most serious and recent competitor to the standard field oriented control (FOC) for induction motors (IM) is the finite control set model predictive control (FCS-MPC). Nevertheless, the extension to multiphase drives faces the impossibility to simultaneously regulate the flux/torque and the secondary current components (typically termed x-y in literature). The application of a single switching state during the whole sampling period inevitably implies the appearance of x-y voltage/currents that increase the system losses and deteriorate the power quality. These circulating currents become intolerably high as the per unit x-y impedance and the switching frequency diminish. Aiming to overcome this limitation, this work suggests the integration of virtual voltage vectors (VVs) into the FCS-MPC structure. The VVs ensure null x-y voltages on average during the sampling period and the MPC approach selects the most suitable VV to fulfill the flux/torque requirements. The experimental results for a six-phase case study compare the standard FCS-MPC with the suggested method, confirming that the VV-based MPC maintains the flux/torque regulation and successfully improves the power quality and efficiency.**

Index Terms*– *Induction Motors, Model Predictive Control, Six-phase drives, Virtual Voltage Vectors.

I. Introduction

Multiphase electric drives were rarely considered at industry and academia in the 20th century. Although relevant works proved the capability of multiphase systems to enhance the fault tolerance and power density of electric drives (by the beginning of the 80s and 90s, respectively), the number of publications and industrial products using more than three phases was still scarce in those days. This situation faced however a turning point with the advent of the 21th century, bringing an incessant growth of the interest on multiphase electric drives since then [1-4]. The last decade has witnessed an exponential increase in the number of publications and the appearance of emblematic applications such as the Queen Elizabeth class aircraft carriers of the Royal Navy [5] (with 80 MW of full-electric ship propulsion using fifteen-phase induction motors) and also in aircraft, high-speed traction and wind energy applications [4].

This re-emergence can be explained by the ever-increasing power of the digital signal processors and power electronic devices together with the creation of a body of knowledge that provides further confidence to replace standard three-phase drives in high-reliability and/or high-power applications [5-9]. Although five- and seven-phase machines have been extensively covered in literature [2-3], the preferred choice at industry is the use of multi three-phase machines that inherit the well-known three-phase technology [5,10-11]. Concurrently with the popularization of multiphase machines and drives, many control techniques that were already well-established in three-phase machines have been extended and generalized to regulate n-phase machines ($n > 3$).

The first of these strategies was the field oriented control (FOC) [12]. In the case of induction machines with distributed windings the extension of FOC to regulate the torque and flux was trivial because the vector space decomposition approach (VSD) showed that the equations in the α-β plane were identical regardless of the number of phases [13]. Consequently, the same cascaded FOC structure used in three-phase drives (with an outer speed loop and two inner d-q current loops) could be equally applied to any n-phase machine. Nevertheless, initial attempts to directly apply three-phase control and modulation strategies disregarding the additional degrees of freedom existing in multiphase systems resulted in highly distorted phase currents and low-performance [14]. The reason is that the x-y components do not affect the torque production (in machines with distributed windings), but allow the flow of low-order current harmonics that increase the copper losses and deteriorate the total harmonic distortion (THD). Aiming to overcome this limitation, both the modulation and the control techniques took into account these additional

Manuscript received January 16, 2017; revised February 20, 2017 and April 17, 2017; accepted May 06, 2017. This work was supported by the Spanish Ministry of Science and Innovation and the European Regional Development Fund under Project ENE2014-52536-C2-1-R.
I. Gonzalez-Prieto, M.J. Duran and J.J. Aciego are with the Department of Electrical Engineering, University of Malaga, Malaga, Spain (e-mail: ignaciogp87@gmail.com, mjduran@uma.es and juanjoseaciego@hotmail.com).
C. Martin and F. Barrero and are with the Department of Electronic Engineering, University of Seville, Seville, Spain (e-mail: cmartin15@us.es and fbarrero@us.es).

components by using additional voltage vectors and currents loops [15]. Some additional complexity was added to the control structure, but the extended FOC proved to satisfactorily regulate multiphase machines [3,12,15].

As it occurred in three-phase drives, other control approaches have appeared as alternative candidates that aim to provide enhanced performance in multiphase drives, especially in terms of robustness, flexibility and fast torque response. Direct torque control (DTC) and sliding mode control (SMC) are two examples of these attempts to dethrone FOC [16-18], but in recent times the main competitor to replace the PI controllers in the inner current loops has been the use of finite-control set model predictive control due to the fast response and flexibility to include restrictions. Initially developed for three-phase systems [19-21], its successful performance led to the consideration of FCS-MPC for multiphase drives [22-29]. These works proved the capability of the standard FCS-MPC approach to regulate multiphase machines using different number of switching states and model approaches. A common feature of all FCS-MPC strategies in [22-29] is however the application of a single switching state during the whole sampling period. Since each switching state simultaneously generates voltage vectors in the α-β and x-y planes, the tracking of the α-β current references to achieve successful speed regulation inevitably leads to the appearance of non-null x-y voltages. This in turn implies that non-zero x-y currents will flow through the stator of the machine, thus spoiling efficiency and power quality. A high switching frequency and a high impedance in the x-y plane limits to some extent this shortcoming, providing successful performance for low-power drives [22-29]. However, as the power of the drive increases the switching frequency of the power switches (typically IGBTs) is limited and the per unit impedance of the stator resistance and leakage inductance decreases. Under these circumstances the use of a single switching state is no longer admissible due to the poor regulation of the x-y currents. Although FCS-MPC includes a cost function that considers both α-β and x-y planes, satisfying the requirements in both subspaces at a minimum desirable level is not feasible: if the weight of the α-β components is high one obtains huge x-y currents and if the weight of the x-y components is increased then the flux and torque regulation provides unacceptable ripple. A first contribution of this work is to highlight and experimentally quantify these shortcomings of standard MPC.

Aiming to solve this problem that uniquely appears in multiphase drives, a second contribution of this work is the use of virtual voltage vectors (VVs) integrated into the FCS-MPC structure in order to limit the injection of x-y currents with acceptable flux/torque generation.. The concept of VVs is the creation of a new averaged voltage vectors by the combination of several switching states during the sampling period. The VVs can be used to increase the resolution of the discrete map of switching combinations but also to cancel out undesirable components [16-17, 31]. In the present case VVs are selected in such a manner that the volt-second x-y components become null, thus ensuring that x-y currents are limited. The FCS-MPC is in charge of the flux/torque regulation of the machine, but the concerns about the x-y currents are eliminated by the use of the VVs. This relief in the regulation of the x-y plane together with the lower number of iterations simplifies the control stage and provides better power quality and lower copper losses.

II. Six-phase IM drive

This section describes the main features of the employed six phase IM drive. An asymmetrical six-phase IM is fed in this work by a dual three-phase voltage source converter (VSC). A simplified scheme of the implemented topology is shown in Fig. 1. The switching state of each VSC leg is defined as S_i, where $S_i = 0$ if the lower switch is ON and the upper switch is OFF, and $S_i = 1$ if the opposite occurs. It is then possible to group the switching states of the VSC as a vector $[S]=\{S_{a1}, S_{b1}, S_{c1}, S_{a2}, S_{b2}, S_{c2}\}$, which identifies the $2^6 = 64$ available switching states. Each stator phase voltage can be in turn obtained from this vector and the dc-link voltage (V_{dc}) as it is stated in (1). Applying the power invariant decoupling Clarke transformation matrix defined in (2) it is then possible to map the phase voltages into two orthogonal stationary subspaces, namely α-β and x-y, plus a zero-sequence component (see Fig. 2, where stator voltage vectors have been identified using a decimal number equivalent to the binary number $[S_{a1}\ S_{b1} S_{c1} S_{a2} S_{b2} S_{c2}]$).

$$[M] = \frac{V_{dc}}{3}\begin{bmatrix} 2 & -1 & -1 & 0 & 0 & 0 \\ -1 & 2 & -1 & 0 & 0 & 0 \\ -1 & -1 & 2 & 0 & 0 & 0 \\ 0 & 0 & 0 & 2 & -1 & -1 \\ 0 & 0 & 0 & -1 & 2 & -1 \\ 0 & 0 & 0 & -1 & -1 & 2 \end{bmatrix} \cdot [S]^T \tag{1}$$

$$[T] = \frac{1}{\sqrt{3}}\begin{bmatrix} 1 & -1/2 & -1/2 & \sqrt{3}/2 & -\sqrt{3}/2 & 0 \\ 0 & \sqrt{3}/2 & -\sqrt{3}/2 & 1/2 & 1/2 & -1 \\ 1 & -1/2 & -1/2 & -\sqrt{3}/2 & \sqrt{3}/2 & 0 \\ 0 & -\sqrt{3}/2 & \sqrt{3}/2 & 1/2 & 1/2 & -1 \\ 1 & 1 & 1 & 0 & 0 & 0 \\ 0 & 0 & 0 & 1 & 1 & 1 \end{bmatrix} \tag{2}$$

$$[v_{as}, v_{\beta s}, v_{xs}, v_{ys}, v_{0+}, v_{0-}]^T = [T] \cdot [v_{a1}, v_{b1}, v_{c1}, v_{a2}, v_{b2}, v_{c2}]^T$$

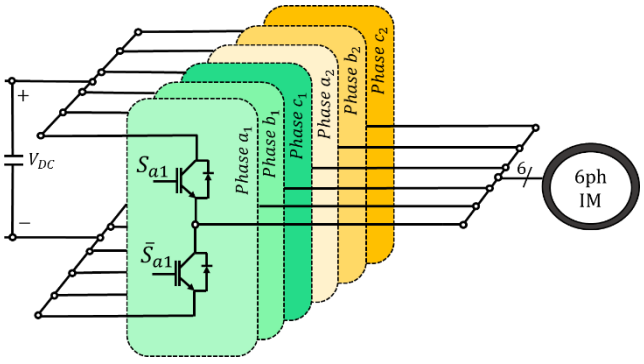

Fig. 1. Scheme of a six-phase IM drive.

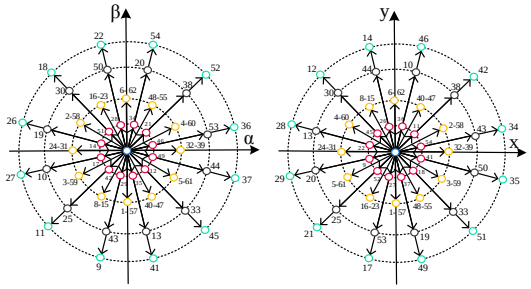

Fig. 2. Voltage space vectors in the α-β and x-y subspaces for a six-phase VSC.

The α-β subspace plays a similar role as in three-phase drives, serving at the control stage to regulate the flux and torque using d and q components, respectively, once the Park transformation is performed:

$$[D] = \begin{bmatrix} cos\theta_s & sin\theta_s \\ -sin\theta_s & cos\theta_s \end{bmatrix}$$
$$[v_{ds}, v_{qs}]^T = [D] \cdot [v_{\alpha s}, v_{\beta s}]^T. \quad (3)$$

The Clarke transformation matrix in (2) allows expressing the equations of the six-phase machine in vector space decomposition (VSD) variables as follows:

$$v_{\alpha s} = \left(R_s + L_s \frac{d}{dt}\right) i_{\alpha s} + M \frac{di_{\alpha r}}{dt}$$
$$v_{\beta s} = \left(R_s + L_s \frac{d}{dt}\right) i_{\beta s} + M \frac{di_{\beta r}}{dt}$$
$$v_{xs} = \left(R_s + L_{ls} \frac{d}{dt}\right) i_{xs}$$
$$v_{ys} = \left(R_s + L_{ls} \frac{d}{dt}\right) i_{ys} \quad (4)$$
$$0 = \left(R_r + L_r \frac{d}{dt}\right) i_{\alpha r} + M \frac{di_{\alpha s}}{dt} + \omega_r L_r i_{\beta r} + \omega_r M i_{\beta s}$$
$$0 = \left(R_r + L_r \frac{d}{dt}\right) i_{\beta r} + M \frac{di_{\beta s}}{dt} - \omega_r L_r i_{\alpha r} - \omega_r M i_{\alpha s}$$
$$T_e = pM\left(i_{\beta r} i_{\alpha s} - i_{\alpha r} i_{\beta s}\right),$$

where p is the number of pole pairs, $L_s = L_{ls} + 3{\cdot}L_m$, $L_r = L_{lr} + 3{\cdot}L_m$, $M = 3{\cdot}L_m$ and ω_r is the rotor electrical speed ($\omega_r = p{\cdot}\omega_m$). Subscripts s and r denote stator and rotor variables, respectively.

The model in VSD variables in (4) can be used in model-based approaches for the prediction of futures states of the drive, as it is detailed in the next section.

III. Model Predictive Control of Six-Phase Induction Motor Drives

The most accepted structure of MPC-based strategies for multiphase drives maintains the outer speed loop with a proportional-integral (PI) controller and replaces the inner current loops using the predictive approach (Fig. 3). The outer speed loop provides the q-current reference while the d-current reference is usually a constant value that is set to provide rated flux in the base-speed region. These d-q currents can be expressed in the α-β subspace using the inverse Park transformation. The objective of these inner current controllers is to track the reference stator currents $i^*_{\alpha\beta xy}$ (Fig. 3). For this purpose, it uses a discrete model of the drive to predict the future behavior of the output variables $\hat{\imath}_{\alpha\beta xy}$. In this work, the machine is modeled using a state-space representation, based on the VSD approach and the dynamic reference transformation. So the predictive model can be given in the following form [29]:

$$\frac{d}{dt}[X_{\alpha\beta xy}] = [A] \cdot [X_{\alpha\beta xy}] + [B] \cdot [U_{\alpha\beta xy}]$$
$$[Y_{\alpha\beta xy}] = [C] \cdot [X_{\alpha\beta xy}] \quad (5)$$

where:

$$[U_{\alpha\beta xy}] = [u_{\alpha s}\ u_{\beta s}\ u_{xs}\ u_{ys}\ 0\ 0]^T$$
$$[X_{\alpha\beta xy}] = [i_{\alpha s}\ i_{\beta s}\ i_{xs}\ i_{ys}\ i_{\alpha r}\ i_{\beta r}]^T \quad (6)$$
$$[Y_{\alpha\beta xy}] = [i_{\alpha s}\ i_{\beta s}\ i_{xs}\ i_{ys}\ 0\ 0]^T$$

The matrices $[A]$, $[B]$ and [C] define the dynamics of a six-phase IM and their coefficients are dependent on the machine parameters, as it is described in [29]. The forward Euler discretization technique is employed to obtain the predictive model. To conclude the analysis of the employed predictive model, it should also be highlighted that the non-measurable variables $i_{\alpha r}$ and $i_{\beta r}$ are estimated using the method C1a from [29]. In this method, all unmeasurable quantities (i.e. rotor variables) are lumped into one term, named G, which is estimated at every sampling instant using past values of the measured variables. This estimation is then introduced in the predictive model to obtain the prediction of the stator currents.

From the point of view of the control process, an optimizer selects the optimal gating signal [S^{opt}] in order to minimize a cost function J_1. The optimization is done by exhaustive search over all possible control signal values. In the case of a six-phase VSC, the 64 voltage vectors can be reduced to 49 independent voltage vectors due to redundancy. For each one of these voltage vectors, the predictive model is computed using the measured speed and stator phase currents to obtain the predicted values of the α-β and x-y currents ($\hat{\imath}_{\alpha\beta xy}$). Then, the cost function value is calculated for all independent switching possibilities and the voltage vector that minimizes the cost function is selected and applied by the VSC during the next sampling period. The cost function must consider the error in the α-β and x-y components as follows:

$$J_1 = K_1 \cdot e_{\alpha s}^2 + K_2 \cdot {e_{\beta s}}^2 + K_3 \cdot {e_{xs}}^2 + K_4 \cdot {e_{ys}}^2 \quad (7)$$

where:

$$e_{\alpha s} = (i^*_{\alpha s} - \hat{\imath}_{\alpha s})$$
$$e_{\beta s} = (i^*_{\beta s} - \hat{\imath}_{\beta s})$$
$$e_{xs} = (i^*_{xs} - \hat{\imath}_{xs}) \quad (8)$$
$$e_{ys} = (i^*_{ys} - \hat{\imath}_{ys}).$$

The K_i coefficients, where $i \in \{1,2,34\}$, are the weighting factors for each component. The value of these coefficients must be selected according to the control objective and drive features. This work deals with a distributed-winding machine and consequently the x-y currents are only a source of copper losses with no impact on the flux/torque production. Hence, the reference value of these currents is usually set to zero and the selection of K_i coefficients is a

tradeoff between flux/torque regulation (K_1 and K_2) and efficiency/distortion (K_3 and K_4). It must be highlighted however that in spite of the possibility to vary the importance that is paid to α-β and x-y planes, the selection of a single switching state S^{opt} (Fig. 3) implies that it is impossible to satisfy the requirements of both planes simultaneously in a sampling period. Further details on the impact of the coefficients tuning on the drive performance are provided in section V.

To sum up, the MPC is a high-performance strategy of control for multiphase drives based on the machine model. As a consequence, it is parameter dependent and computationally intensive, but it also inherits the advantages that have been extensively highlighted in three-phase drives (fats torque response, flexibility and simplicity, to name a few).

IV. Model Predictive Control Using Virtual Voltage Vectors

This section describes the implementation of the proposed MPC based on the utilization of VVs that aims to improve the performance of the standard MPC. For this purpose, the first step is to analyze the space voltage vectors in the α-β and x-y subspaces for a six-phase VSC.

Fig. 2 shows that the voltage vectors in six-phase machines can be classified in small, medium, medium-large and large voltage vectors in α-β and x-y planes. Medium-large vectors in the α-β plane result in medium-large vectors in the x-y plane. However, large vectors in the α-β plane are turned into small vectors in the x-y plane and vice versa. Moreover, medium-large and large vectors with same direction in the α-β plane have opposite direction in the x-y plane (see Fig. 2). Taking advantage of this fact, VVs can be created to reduce harmonic components in the x-y plane. These VVs are obtained with one medium-large and one large voltage vector (see Fig. 4) that must generate zero average voltage in the x-y plane. For this purpose, a different application time of the medium and large voltage vector is necessary. For example, VV_1 is formed by the voltage vector V_{53} (medium-large voltage vector in the α-β plane) and V_{36} (large voltage vector in the α-β plane) with different application times t_2 and t_1, respectively, to provide a zero average voltage vector in the x-y plane. In a six-phase VSC, the application time of each voltage vector must be t_1=0.73 · T_m and t_2=0.27 · T_m.

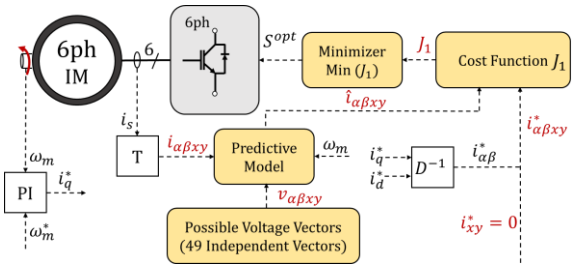

Fig. 3. MPC scheme for a six-phase IM drive.

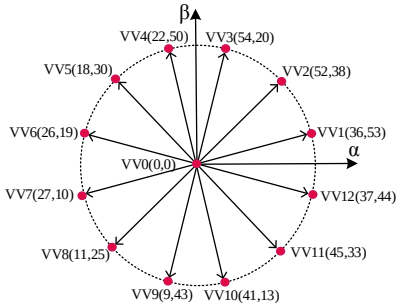

Fig. 4. Applied VVs in the analyzed six-phase drive and α-β subspace.

Therefore, the general form of the VVs is the following:

$$VV_i = t_1 \cdot V_{large} + t_2 \cdot V_{medium-large} \quad (9)$$

The implementation of these VVs in a MPC strategy intrinsically provides zero average value of the x-y components with no inclusion of these components into the control strategy. This fundamental advantage is possible because the VV-MPC uses two voltage vectors in each sample time whereas the standard MPC only employs a single voltage vector. It must be highlighted however that the size of the VVs is 7.2% smaller than the size of the large vectors, and this diminishes to some extent the utilization of the dc-bus voltage. As in overmodulation techniques in space vector PWM [30], it is possible to transit from VVs to single large vectors in order to fully exploit the dc-link voltage, but this procedure is not covered in this work.

In addition to the key feature of nullifying x-y voltage components, the utilization of the VVs provides some further simplifications in the control strategy that eases its implementation compared to the standard MPC from Fig. 3. These modifications in the VV-MPC control strategy are shown in green color in the control diagram of Fig. 5. For example, the predictive model of (5) can be reduced due to the absence of x-y components in the model. Hence, a new reduced predictive model can be defined as:

$$\begin{aligned} \frac{d}{dt}[X_{\alpha\beta}] &= [\bar{A}] \cdot [X_{\alpha\beta}] + [\bar{B}] \cdot [U_{\alpha\beta}] \\ [Y_{\alpha\beta}] &= [\bar{C}] \cdot [X_{\alpha\beta}] \end{aligned} \quad (10)$$

where:

$$\begin{aligned} [U_{\alpha\beta}] &= [u_{\alpha s}\ u_{\beta s}\ \ 0\ 0]^T \\ [X_{\alpha\beta}] &= [i_{\alpha s}\ i_{\beta s}\ \ i_{\alpha r}\ i_{\beta r}]^T \\ [Y_{\alpha\beta}] &= [i_{\alpha s}\ i_{\beta s}\ \ 0\ 0]^T \end{aligned} \quad (11)$$

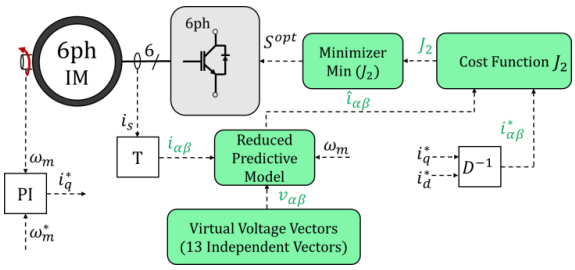

Fig. 5. VVs based MPC scheme for a six-phase IM drive.

In addition to the reduction of the model size, the utilization of a reduced number of voltage vectors diminishes the number of iterations and the computational cost of the method. Finally, the cost function can also be simplified by eliminating the x-y terms:

$$J_2 = K_1 \cdot e_{\alpha s}^2 + K_2 \cdot {e_{\beta s}}^2 \quad (12)$$

In summary, the implementation of the VVs in a MPC strategy provides the following advantages from the point of view of the control process:

i) Utilization of a reduced predictive model where the x-y components are not present.

ii) Use of a new cost function without the e_{xs}-e_{ys} terms.

iii) Reduction of the number of K_i coefficients that must be calculated in the cost function and reduction in the number of iterations that need to be performed each sampling time (from 49 to 13).

It must be highlighted that generating null x-y voltages might lead to non-zero x-y currents due to the dead-time effect or asymmetries in the system. However, including non-null x-y voltages in open-loop mode to cancel x-y currents would highly increase the complexity of the approach. This work assumes that the system is reasonably symmetric and the injection of x-y currents is sufficiently small to obtain good performance. The next section experimentally confirms the performance of the proposed VV-MPC and its capability to limit x-y currents significantly compared to standard MPC.

V. Experimental Results

A. Test Bench

Fig. 6 shows the elements of the test bench that has been used for the experimental testing. The six-phase drive consists of an asymmetrical six-phase IM supplied from conventional two-level three-phase VSCs (Semikron SKS22F modules). The parameters of the custom-built six-phase IM have been obtained using ac-time domain and stand-still with inverter supply tests [32-33]. Table I shows the induction motor drive parameters and rated values.

TABLE I
Induction Motor Drive Parameters and Test-bench Rated Values

Power (kW)	0.8
Dc-link voltage (V)	200
Dead time (μs)	4
I_{peak} (A)	4.06
i_d (A)	0.8
i_q (A)	7
n_m (rpm)	1000
R_s (Ω)	4.2
R_r (Ω)	2
L_m (mH)	420
L_{ls} (mH)	1.5
L_{lr} (mH)	55

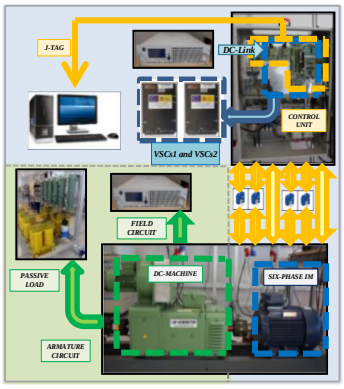

Fig. 6. Test bench

A single dc power supplies the VSCs and the control actions are performed by a digital signal processor (TMS320F28335 from Texas Instruments, TI). The control unit is programmed using a JTAG and the TI proprietary software called Code Composer Studio. The current and speed measurements are taken with four hall-effect sensors (LEM LAH 25-NP) and a digital encoder (GHM510296R/2500), respectively. The six-phase IM is loaded coupling to the shaft to a dc machine that acts as a generator. The armature of the dc machine is connected to a variable passive *R* load that dissipates the power and the load torque is consequently speed-dependent.

B. Experimental Results

The performance of the proposed VV-MPC and the standard MPC are compared next in steady-state and transients. In both strategies the switching frequency is variable because the switching state of the six VSC legs is not changed in every sampling period, as it typically occurs in pulse-width modulation (PWM) [34-35]. The switching frequency of VV-MPC is in general somewhat higher than MPC for the same sampling period. The experimental results compare MPC at $100\mu s$ with VV-MPC at $100\mu s$ and VV-MPC at $200\mu s$, so that the switching frequency of MPC is in between the switching frequency of the other VV-MPC tests. The *d*-current reference is set to 0.8A and the weighting factors that regulate α-β currents are set to K_1=K_2=1 in all tests. The values of K_1 and K_2 can be set arbitrarily since the MPC and VV-MPC select the switching state (or virtual vector) that provide better current tracking regardless of the multiplying factor. What is relevant is the proportion of the x-y weighting factors (K_3-K_4) to the α-β weighting factors (K_1-K_2) because this ratio defines the importance that is given to each plane. The weighting factors have been obtained on an empirical basis following a trial and error procedure that considers that K_3-K_4 should provide a good compromise between the current tracking in both α-β and x-y planes (as it is shown next in Fig. 7).

A first test (Fig. 7) verifies the inability of MPC to regulate the x-y currents regardless of how the weighting factors K_3 and K_4 are tuned. The reference speed is changed from 200 to 300 rpm at $t = 5s$ in a ramp-wise manner in order to also

verify the dynamic performance. In the results shown in the left side of Fig. 7 a low value for the x-y weighting factors is set (K_3=K_4=0.001), obtaining a good speed and d-q current tracking (Fig. 7a-7b), but a poor regulation of the x-y currents (Fig. 7c). A lower value of the weighting factors K_3-K_4 further deteriorates the x-y current tracking while the margin to improve the α-β current tracking is narrow. An attempt to improve the regulation of x-y currents is shown in the middle plots of Fig. 7, where the weighting factor of the x-y currents is increased up to K_3=K_4=0.075. Unfortunately, while the x-y currents remain large, paying more attention to the x-y plane compromises the flux/torque regulation and deteriorates the d-q current tracking (Fig. 7b). Comparing the left and middle plots in Fig. 7, the THD of the α-β currents is increased from 10.2 to 15.8% and this affects the flux/torque regulation. On the other hand the x-y currents cannot be reduced and the copper losses are increased by 28%. The tuning of K_3 and K_4 cannot change the fact that a single switching state always generates x-y voltages, those being the main cause of the high x-y currents shown in Fig. 7. A first contribution of this work is to highlight the limitation of standard MPC [22-29] to simultaneously limit the x-y currents and obtain low-ripple d-q currents when the impedance of the x-y plane is rather low. Right plots in Fig. 7 finally show the results of the proposed VV-MPC strategy. While the speed and d-q tracking is mostly similar to that of the MPC, the regulation of the x-y currents is significantly improved using the VV-MPC approach thanks to the zero volt-second x-y voltages provided by the VVs (Fig. 7c). A second contribution is the proposal of the VV-MPC method to successfully limit x-y currents while retaining a similar dynamic performance as in MPC.

A second test (Fig. 8) verifies the steady-state performance setting a constant target speed of 300 rpm. Comparing MPC (left plots) and the proposed VV-MPC (middle plots), it can be observed that the speed regulation (Fig. 8a) and the d-q current tracking (Fig. 8b) is also satisfactory in both approaches. A significant difference is obtained however in terms of the x-y current regulation. While the MPC provides large x-y currents (Fig. 8c, left), the use of the VVs clearly limits the amount of x-y currents (Fig. 8c, middle). The inability of the MPC to regulate the x-y currents in turn results in a low power quality of the stator currents (Fig. 8d, left). On the contrary, the cancelation of the x-y voltages in the VV-MPC improves the power quality of the phase currents and reduces the stator copper losses. This can be observed at a glance in Fig. 8d. The THD is reduced by 83% and the copper losses are reduced by 42%, this being a significant improvement in terms of current distortion and efficiency of the drive. In order to test the goodness of the proposed VV-MPC at lower switching frequencies, the right plots in Fig. 8 show the same tests but using a double sampling period ($200\mu s$) for the VV-MPC strategy. The switching frequencies of MPC at $100\mu s$, VV-MPC at $100\mu s$ and VV-MPC at $200\mu s$ are 3840 Hz, 5140 Hz and 2756 Hz, respectively, thus confirming that the switching frequency of MPC is in between that of the VV-MPC-based tests. The current ripple both in α-β and x-y planes is slightly increased but the speed tracking is good and the x-y currents remain limited compared to the standard MPC.

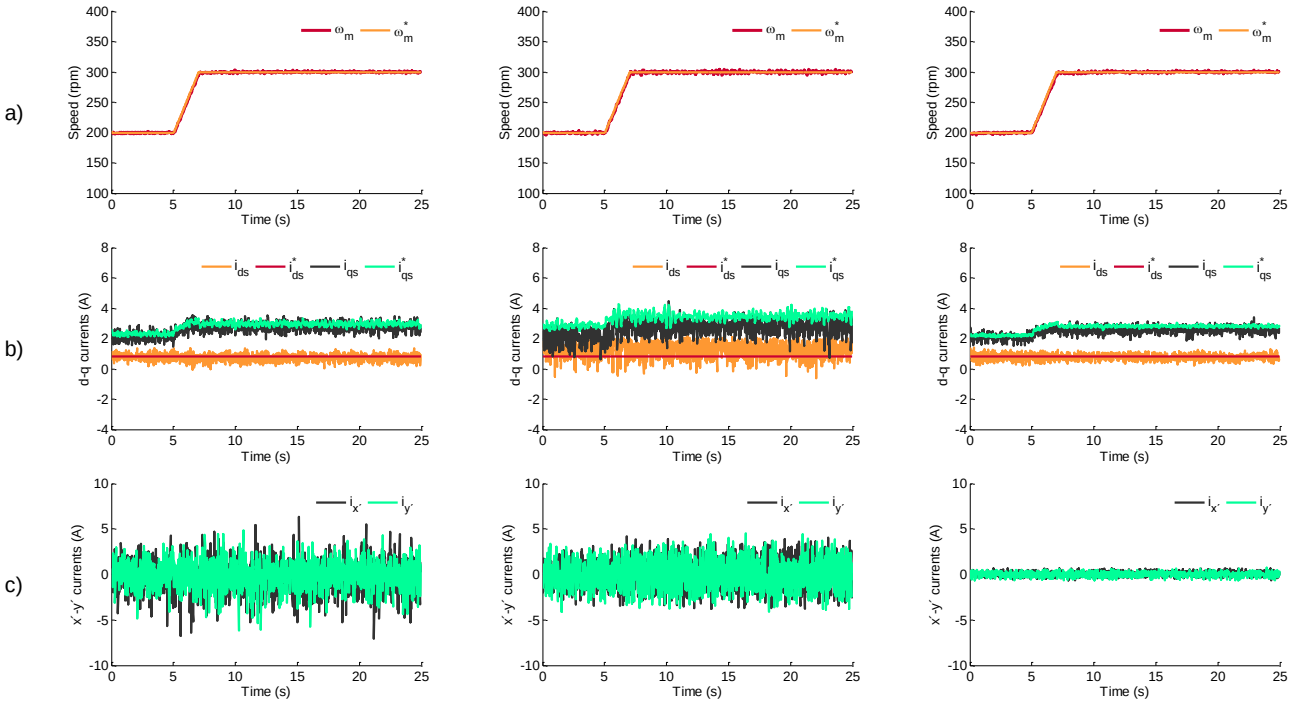

Fig. 7. Test 1 for MPC with K_3=K_4=0.001 (left plots), MPC with K_3=K_4=0.0075 (middle plots) and VV-MPC (right plots). From top to bottom: a) Motor speed, b) *d-q* currents and c) *x-y* currents.

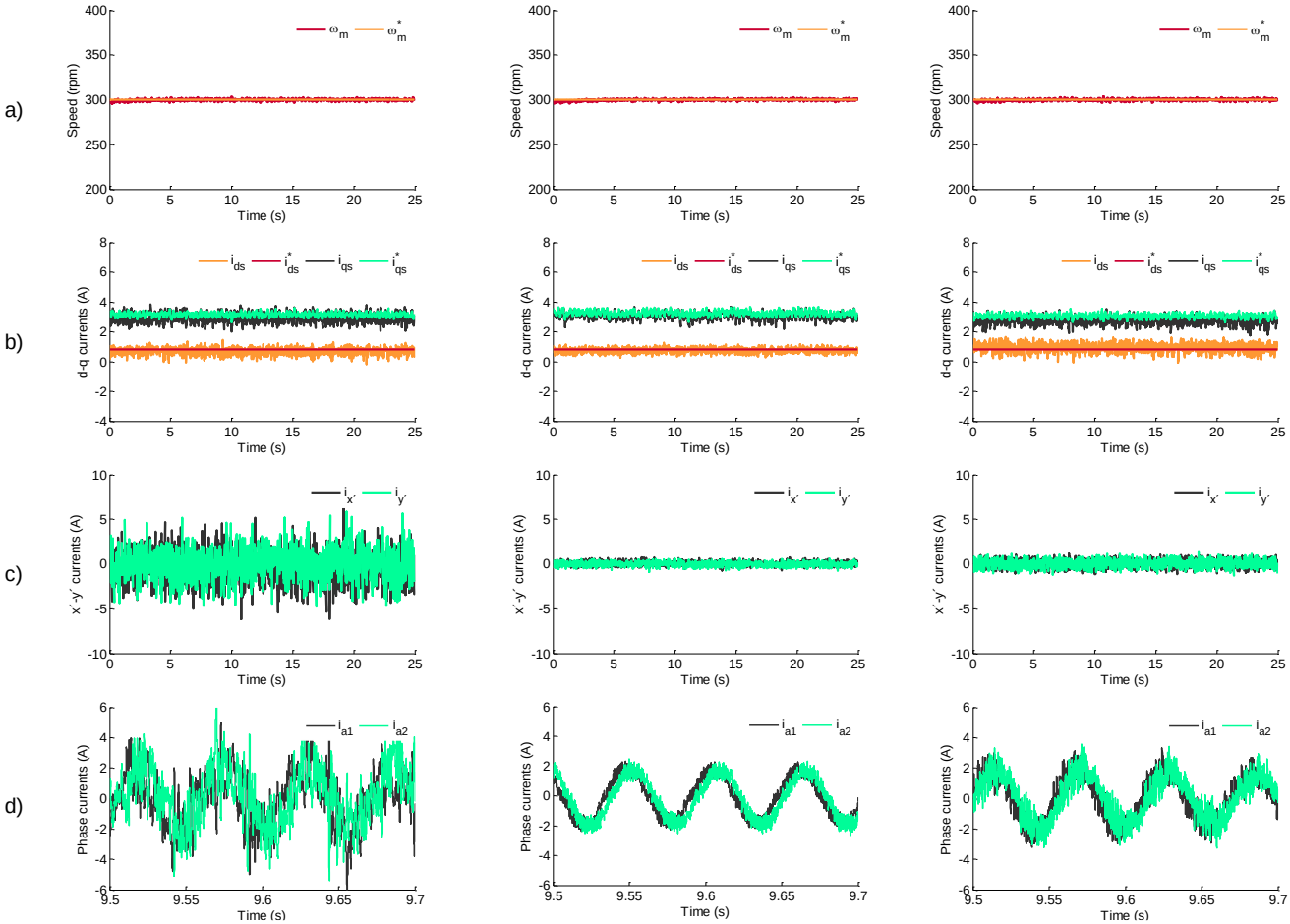

Fig. 8. Test 2 for MPC with $T_s = 100\mu s$ (left plots), VV-MPC with $T_s = 100\mu s$ (middle plots) and VV-MPC with $T_s = 200\mu s$ (right plots). From top to bottom: a) Motor speed, b) *d-q* currents, c) *x-y* currents and d) a_1-a_2 phase currents.

It is remarkable that VV-MPC at $200\mu s$ provides lower current ripple than conventional MPC at $100\mu s$ with lower switching frequency. Since VV-MPC and MPC are methods of a different kind with a different selection of the switching states, it is possible to simultaneously decrease the switching frequency and at the same time obtain a significant improvement in the phase current ripple. The reason for this is that the average x-y voltage is zeroed in VV-MPC and, consequently, the average x-y currents are reduced.

For better visualization of the improvement that is obtained in terms of distortion, Fig. 9 depicts the frequency spectrum of phase currents for the three methods considered so far: MPC at $100\mu s$ (Fig. 9a), VV-MPC at $100\mu s$ (Fig. 9b) and VV-MPC at $200\mu s$ (Fig. 9c). As it is well-known, the spectrum in the MPC approach is spread (Fig. 9a), this being different compared to PWM-based control where the current harmonics are located in specific frequencies. There is however a significant amount of low order harmonics (see zoom-in plot in Fig. 9a) that are responsible for the distorted waveform shown in Fig. 8d. The spectrum in VV-MPC (Figs. 9b and 9c) is also spread, but it is visible that the amount of current harmonics is drastically reduced.

A load rejection test is finally included in a third test (Fig. 10) to further verify that the VV-MPC retains the performance of MPC in terms of flux/torque regulation but offers a better regulation of the x-y currents. The motor is driven at 300 rpm with a load torque of 2 Nm and this load is stepped down to 0.75 Nm at time $t = 9.5s$ (Fig. 10b). The deloading transiently accelerates the six-phase induction motor, but the control action brings the speed back to the reference speed of 300 rpm with a similar performance in both MPC and VV-MPC approaches (Fig. 10a). As in the former tests, the d-q current tracking is similar in all cases (Fig. 10c) whereas the power quality is highly improved using the VV-MPC strategy (Fig. 10d). Fig. 9e shows the α-β currents during the transient to confirm that the tracking in this plane is satisfactorily achieved using MPC. Nevertheless, the main issue in MPC remains to be the poor regulation of the x-y currents that results in highly distorted phase currents (Fig. 10f).

A fourth test is finally included in Fig. 11 to verify the performance of MPC and VV-MPC for different operating points. A total amount of eighteen tests have been performed, nine for MPC (top surfaces in Fig. 11) and nine for VV-MPC (bottom surfaces in Fig. 11). Each of the nine tests for each method have been done considering three target speed values (200, 350 and 500 rpm) and three values of the resistance that is connected to the dc generator (20, 30 and 40 Ω) t hat provide different amount of load torque (ranging from 2 Nm to 6.8 Nm). Fig. 11a shows that the rms

value of the phase currents is lower in VV-MPC compared to standard MPC in the whole range of operation that is explored. This in turn implies that the stator copper losses are reduced using VV-MPC in a range between 54% and 20%. Fig. 11b depicts the phase current THD for both methods, showing a reduction of the THD with VV-MPC that ranges between 85 % to 75 %. Results from Fig. 11 just confirm that the improvement in terms of quality and copper losses that has been illustrated in Figs. 7-10 is general for different operating points, further confirming the goodness of the proposal.

To sum up, the proposed VV-MPC overcomes the limitations of MPC in terms of x-y current regulation providing improved quality of the stator currents. This enhanced performance is obtained while retaining the capability of MPC to regulate the speed in steady-state and dynamic conditions.

VI. Conclusion

Although model predictive control is a promising strategy to achieve a fast torque response with a simple and flexible structure, its extension to multiphase drives faces the impossibility to simultaneously satisfy the requirements of the newly appeared subspaces. As a consequence, the selection of a single switching state in MPC inevitably results in high x-y currents. This shortcoming can be however eliminated combining more than one switching state in order to cancel out the x-y voltages. For this purpose, some predefined virtual vectors can be set in advance and be later on included in a model predictive control scheme. The proposed scheme becomes simpler because the control is relieved to regulate the x-y plane and a lower number of iterations is required. In spite of the additional simplicity, the regulation of x-y currents is highly improved and this leads to lower copper losses and better power quality.

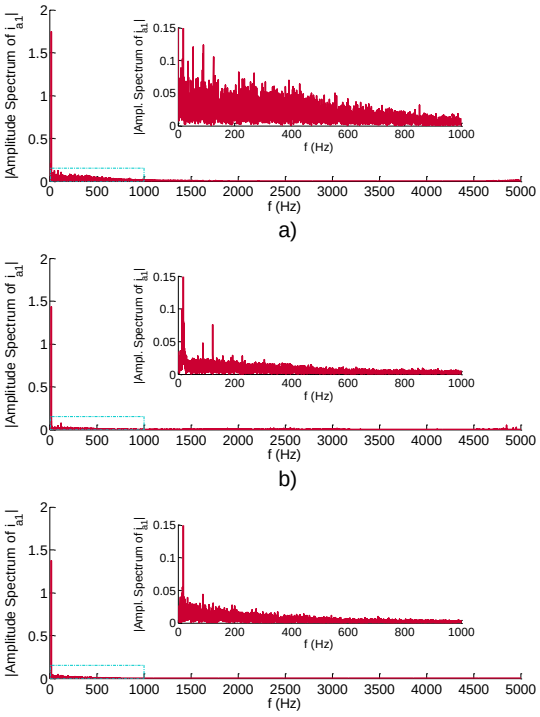

Fig. 9. Frequency spectrum of phase currents for MPC with $T_s = 100\mu s$ (top plot), VV-MPC with $T_s = 200\mu s$ (middle plot) and VV-MPC with $T_s = 100\mu s$ (bottom plot) in the Test 2.

References

[1] E. Levi, F. Barrero and M.J. Duran, "Multiphase machines and drives – Revisited," *IEEE Trans. Ind. Electron.*, vol 63, no. 1, pp. 429-432, 2016.

[2] E. Levi, "Advances in converter control and innovative exploitation of additional degrees of freedom for multiphase machines," *IEEE Trans. on Ind. Electron.*, vol 63, no. 1, pp. 433-448, 2016.

[3] F. Barrero and M.J. Duran, "Recent advances in the design, modeling and control of multiphase machines – Part 1," *IEEE Trans. on Ind.l Electron.*, vol 63, no. 1, pp. 449-458, 2016.

[4] M.J. Duran and F. Barrero, "Recent advances in the design, modeling and control of multiphase machines – Part 2," *IEEE Trans. on Ind. Electron.*, vol 63, no. 1, pp. 459-468, 2016.

[5] http://www.aircraftcarrieralliance.co.uk/the-ships/the-queen-elizabeth-class.aspx [Online available] 2017.

[6] A. Cavagnino, Z. Li, A. Tenconi and S. Vaschetto, "Integrated generator for more electric engine: design and testing of a scaled-size prototype," *IEEE Trans. Ind. Appl.*, vol. 49, no. 5, pp. 2034-2043, 2013.

[7] H.S. Che, E. Levi, M. Jones, M.J. Duran, W.P. Hew and N.A. Rahim, "Operation of a six-phase induction machine using series-connected machine-side converters," *IEEE Trans. on Ind. Electron.*, vol. 61, no. 1, pp. 164-176, 2014.

[8] I. Gonzalez-Prieto, M.J. Duran, F. Barrero, M. Bermudez and H. Guzman, "Impact of post-fault flux adaptation on six-phase induction motor drives with parallel converters," *IEEE Trans. on Power Electron.*, vol. 32, no. 1, pp. 515-528, 2017.

[9] G. Sulligoi, A. Tessarolo, V. Benucci, A.M. Trpani, M. Baret and F. Luise, "Design and development of a medium-voltage dc generation system," *IEEE Ind. Appl. Mag.*, vol. 19, no. 4, pp. 47-55, 2013.

[10] E. Jung, H. Yoo, S. Sul, H. Choi and Y. Choi, "A nine-phase permanent-magnet motor drive system for an ultrahigh-speed elevator," *IEEE Trans. on Ind. Appl.*, vol. 48, no. 3, pp. 987-995, 2012.

[11] Gamesa Technological Corporation S.A. (2016, Oct 25). *Gamesa 5.0 MW* [Online]. Available: http://www.gamesacorp.com/recursos/doc/productos-servicios/aerogeneradores/catalogo-g10x-45mw.pdf

[12] E. Levi, R. Bojoi, F. Profumo, H.A. Toliyat and S. Williamson, "Multiphase induction motor drives - A technology status review," *IET Elec. Power Appl.*, vol. 1, no. 4, pp. 489-516, 2007.

[13] Y. Zhao and T.A. Lipo, "Space vector PWM control of dual three-phase induction machine using vector space decomposition', *IEEE Trans. Ind. Appl.*, vol. 31, no.5, pp. 1100–1109, 1995.

[14] H.A. Toliyat, R. Shi, and H. Xu, "A DSP-based vector control of five-phase synchornous reluctance motor," in Proc. IEEE Ind. Applications Society Annual Meeting IAS Rome, *Italy*, 2000, CD-ROM Paper No. 40_05.

[15] R. Bojoi, E. Levi, F.Farina, A. Tenconi, and F. Profumo, "Dual three-phase induction motor drive with digital current control in the stationary reference frame," *IEE Proc. Electr. Power Appl.*, vol. 153, no. 1, pp. 129–139, 2006.

[16] L. Zheng, J.E. Fletcher, B.W. Williams and X. He, "A Novel Direct Torque Control Scheme for a Sensorless Five-Phase Induction Motor Drive," *IEEE Trans. on Ind. Electron.*, vol. 58, no. 2, pp. 503-513, 2011.

[17] M. Bermudez, I. Gonzalez-Prieto, F. Barrero, H. Guzman and M.J. Duran; Xavier Kestelyn" Open-Phase Fault-Tolerant Direct Torque Control Technique for Five-Phase Induction Motor Drives," *IEEE Trans. on Ind. Electron.*, vol. 64, no. 2, pp. 902-911, 2017.

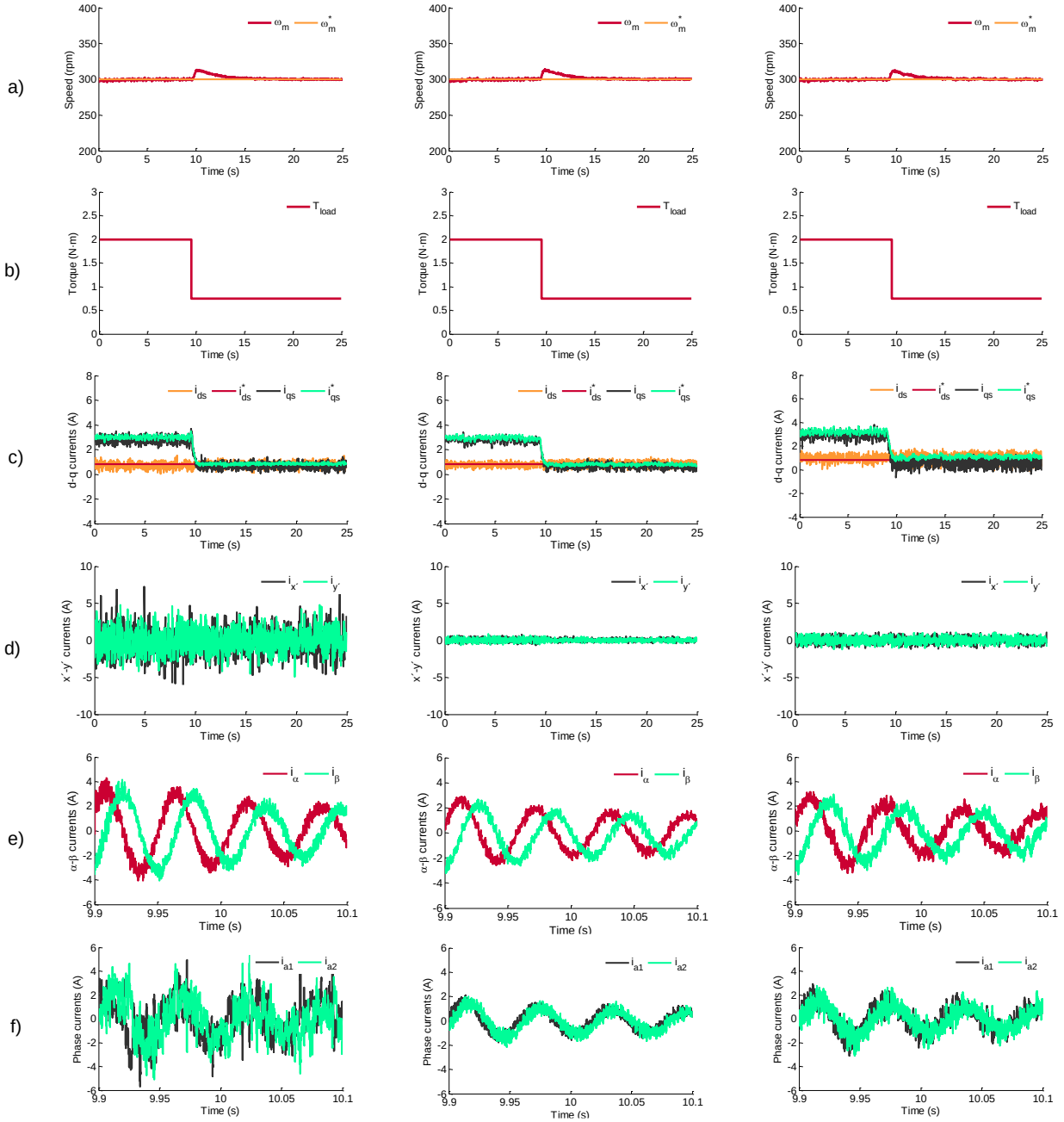

Fig. 10. Test 3 for MPC with $T_s = 100\mu s$ (left plots), VV-MPC with $T_s = 100\mu s$ (middle plots) and VV-MPC with $T_s = 200\mu s$ (right plots). From top to bottom: a) Motor speed, b) load torque, c) *d-q* currents, d) *x-y* currents, e) α-β currents and f) a_1-a_2 phase currents.

[18] M.A. Fnaiech, F. Betin, G.A. Capolino and F. Fnaiech, "Fuzzy logic and sliding-mode controls applied to six-phase induction machine with open phases," *IEEE Trans. Ind. Electron.*, vol. 57, no. 1, pp. 354-364, 2010.

[19] S. Kouro, P. Cortes, R. Vargas, U. Ammann and J. Rodriguez, " Model Predictive Control—A Simple and Powerful Method to Control Power Converters," *IEEE Trans. Ind. Electron.*, vol. 56, no. 6, pp. 1826-1838, 2009.

[20] J. Rodriguez, R.M. Kennel, J.R. Espinoza, M. Trincado, C.A. Silva and C.A. Rojas, "High-Performance Control Strategies for Electrical Drives: An Experimental Assessment," *IEEE Trans. on Ind. Electron.*, vol. 59, no. 2, pp. 812-820, 2012

[21] E. Fuentes, D. Kalise, J. Rodríguez and R.M. Kennel, " Cascade-Free Predictive Speed Control for Electrical Drives," *IEEE Trans. Ind. Electron.*, vol. 61, no. 5, pp. 2176-2184, 2014.

[22] C. Lim, E. Levi, M. Jones, N. Abd Rahim and W. Hew, "FCS-MPC Based Current Control of a Five-Phase Induction Motor and its Comparison with PI-PWM Control," *IEEE Trans. on Ind. Electron.*, vol. 61, no. 1, pp. 149-163, 2014.

[23] C. Lim, E. Levi, M. Jones, N. Abd Rahim and W. Hew, "A Comparative Study of Synchronous Current Control Schemes Based on FCS-MPC and PI-PWM for a Two-Motor Three-Phase Drive," *IEEE Trans. on Ind. Electron.*, vol. 61, no. 8, pp. 3867-3878, 2014.

[24] M.R. Arahal, F. Barrero, S. Toral, M.J. Durán and R. Gregor, "Multi-phase Current Control Using Finite–state Model-Predictive Control," *Control Eng. Pract.*, vol. 17, no. 5, pp. 579-587, 2009.

[25] F. Barrero, M.R. Arahal, R. Gregor, S. Toral and M.J. Duran, "A Proof of Concept Study of Predictive Current Control for VSI Driven Asymmetrical Dual Three-phase AC Machines," *IEEE Trans. on Ind. Electron.*, vol. 56, no. 6, pp. 1937-1954, 2009.

a)

b)

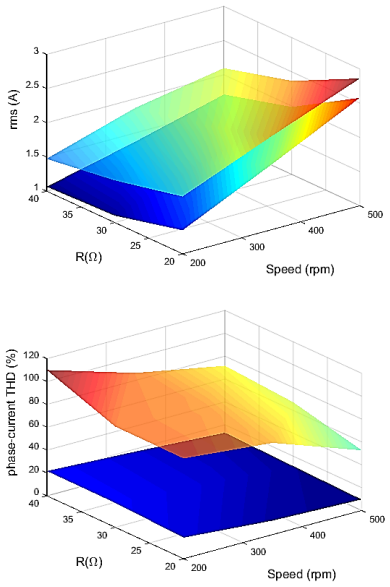

Fig. 11. Test 4 showing the performance of MPC (top surface) and VV-MPC (bottom surface) for different steady-state operating points: a) rms value of the phase currents and b) THD value of the phase currents.

[26] M.J. Duran, J. Prieto, F. Barrero and S. Toral, "Predictive Current Control of Dual Three-phase Drives using Restrained Search Techniques," *IEEE Trans. on Ind. Electron.*, vol. 58, no. 8, pp. 3253-3263, 2011.

[27] J. Riveros, F. Barrero, E. Levi, M.J. Durán, M. Jones and S. Toral, "Variable-Speed Five-Phase Induction Motor Drive Based on Predictive Torque Control," *IEEE Trans. on Ind. Electron.*, vol. 60, no. 8, pp. 2957-2968, 2013.

[28] R.S. Arashloo, M. Salehifar, J.L. Romeral and V. Sala, " Fault-tolerant model predictive control of five-phase permanent magnet motors," *in proc. of IECON 2013 - 39th Annual Conference of the IEEE Industrial Electronics Society*, pp. 2857-2862, Vienna, Austria, 2013.

[29] C. Martín, M.R. Arahal, F. Barrero and M.J. Duran, " Five-Phase Induction Motor Rotor Current Observer for Finite Control Set Model Predictive Control of Stator Current," *IEEE Trans. on Ind. Electron.*, vol. 63, no. 7, pp. 4527-4538, 2016.

M.J. Duran, J. Prieto, and F. Barrero, "Space vector PWM with reduced common-mode voltage for five-phase induction motor drives operating in overmodulation zone," *IEEE Trans. on Power Electron.*, vol. 28, no. 8, pp. 4030-4040, 2013.

[30] S. Vazquez, J.I. Leon, L.G. Franquelo, J.M. Carrasco, O. Martinez, J. Rodriguez, P. Cortes and S. Kouro, " Model Predictive Control with constant switching frequency using a Discrete Space Vector Modulation with virtual state vectors," *in proc. of the IEEE International Conference on Industrial Technology*, 2009.

[31] A. Yepes, J.A. Riveros, J. Doval-Gandoy, F. Barrero, O. Lopez, B. Bogado, M. Jonesa and E. Levi, "Parameter identification of multiphase induction machines with distributed windings-part 1: sinusoidal excitation methods," *IEEE Trans. on Energy Conv.*, vol. 27, no. 4, pp. 1056-1066, 2012.

[32] J.A. Riveros, A. Yepes, F. Barrero, J. Doval-Gandoy, B. Bogado, O. Lopez, M. Jones and E. Levi, "Parameter identification of multiphase induction machines with distributed windings-part 2: time-domain techniques," *IEEE Trans. on Energy Conv.*, vol. 27, no. 4, pp. 1067-1077, 2012.

[33] A. Tani, M. Mengoni, L. Zarri, G. Serra and D. Casadei, "Control of multiphase induction motors with an odd number of phases under open-circuit phase faults," *IEEE Trans. on Power Electron.*, vol. 27, no. 2, pp. 565-577, 2012.

[34] A.S. Abdel-Khalik, S. Ahmed and A.M. Massoud, "A Nine-Phase Six-Terminal Concentrated Single Layer Winding Layout for High-Power Medium-Voltage Induction Machines," *IEEE Trans. on Ind. Electron.*, early access, 2017.

Ignacio González Prieto was born in Malaga, Spain, in 1987. He received the Industrial Engineer and M.Sc. degrees in fluid mechanics from the University of Malaga, Malaga, Spain, in 2012 and 2013, ´ respectively, and the Ph.D. degree in electronic engineering from the University of Seville, Sevilla, Spain, in 2016. His research interests include multiphase machines, wind energy systems, and electrical vehicles

Mario J. Duran was born in Malaga, Spain, in 1975. He received the M.Sc. and Ph.D. degrees in electrical engineering from the University of Malaga, Malaga, in 1999 and 2003, respectively. He is currently an Associate Professor in the Department of Electrical Engineering, University of Malaga. His research interests include modeling and ´ control of multiphase drives and renewable energies conversion systems.

Juan J. Aciego was born in Málaga, Spain, in 1976.He received the Industrial Engineer and M.Sc. degrees from the University of Malaga, Malaga, Spain, in 2010 and 2016, respectively. He is currently working toward the Ph.D. degree in the Department of Electrical Engineering.
His research interests include power modeling and control of multiphase drives, renewable energy conversion systems and electric vehicles.

Cristina Martín was born in Seville, Spain, in 1989. She received the Industrial Engineer degree from the University of Málaga, Spain, in 2014. In 2015, she joined the Electronic Engineering Department of the University of Seville, where she is currently working toward the Ph.D. degree. Her current research interests include modeling and control of multiphase drives, microprocessor and DSP device systems, and electrical vehicles.

Federico Barrero (M 04; SM 05) received the MSc and PhD degrees in Electrical and Electronic Engineering from the University of Seville, Spain, in 1992 and 1998, respectively. In 1992, he joined the Electronic Engineering Department at the University of Seville, where he is currently a Full Professor. He received the Best Paper Awards from the IEEE Trans. on Ind. Electron. for 2009 and from the IET Electric Power Applications for 2010-2011.